4. Other Research

Li^+ affinity of C_2H_3 and C_2H_5 radicals: ab initio characterization of Li^+-radical complexes

Contact Person Toshihiro Fujii
Environmental Chemistry Devision
National Institute for Environmental Studies

Research Organization
Special Research Projects
Theme Studies on exposure to halogenated organic compounds and its human health effects

Researchers H. Ichikawa (Guest Scientist from Hoshi College of Pharmacy)
H. Shinoda (Guest Scientist from Toyama Medical and Pharmaceutical University)
Y. Soma (Regional Environmental Division)

Keywords ab initio MO, Li^+ affinity, free radical

In our experiments of Li^+ ion attachment/mass spectrometry (1), hydrocarbon free radicals (R) are attached by lithium cations Li^+ and their adduct ions (RLi^+) are measured mass spectrometrically (2,3). Almost nothing was known about such cation-radical adducts and their nature of the bonding. Understanding of Li^+ ion attachment process forming RLi^+ will require parallel theoretical efforts to clarify energetic properties of Li^+ ion, free radicals and Li^+ adduct complexes. In this sense, ab initio molecular orbital calculations help at providing some important insight into the factors such as binding energies, charge distributions, geometrical distortions and the intrinsic interaction between organic radical and Li^+ ion.

Very recently, motivated by the Fujii's experiments (2), Bentley (4) reported the theoretical study of lithium cation interactions with hydrocarbon radicals. To our knowledge, this is only one prior theoretical report on such topics. His essential conclusion is that the bonding between lithium cations and hydrocarbon (HC) radicals appears to be governed by the same electrostatic interactions that stabilize Li^+ interactions with cloced-shell molecules. According to his calculation, the stabilization energies of C_2H_3-Li^+ are on the order of 1 eV, very different from that of our preliminary MO work.(2) This apparent difference should be examined.

The method used is essentially the same methods as those appeared in numerous theoretical literatures (5,6,7,8) for adducts formed between the alkali ions (or proton) and neutral closed-shell molecules.

This paper reports the determination of Li^+ affinities of C_2H_3 and C_2H_5 radicals. Studies include the equilibrium structure at the electronic ground state, the influence of diffuse function, electron correlation, zero-point energy (ZPE) and basis set superposition error (BSSE) and the relative importance of covalent vs electrostatic bonding for Li^+ with C_2H_3 or C_2H_5. The objectives is to give some guide to the interpretation of (i) experimental topics of lithium-ion attachment to the radical species in the gas phase, (ii) related topics of the measurements of Li^+ affinity for a number of neutral, closed-shell molecules (9,10,11) and (iii) the difference between the radical (open-shell) and closed-shell adducts. We believe that the determination of Li^+ affinity of radicals will be essential in future development of Li^+ ion attachment/mass spectrometry technique for radical detection.

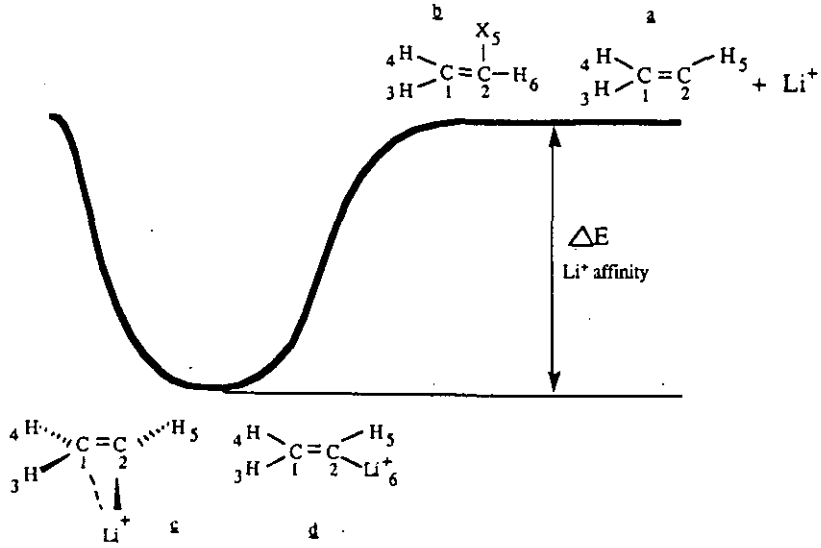

Computational Details

All calculations were performed within the framework of the Gaussian 90 system (12) using the basis sets incorporated in this system to calculate an equilibrium structure and the total energy E. The standard 6-31G** basis sets were mainly employed in the calculation. The geometries are optimized at the self-consistent-field (SCF) level by using analytical first and second-derivative techniques. Spin-restricted Hartree Fock (RHF) theory is used for closed-shell Li^+ ion and spin-unrestricted Hartree Fock (UHF) for the neutral and cation radicals. We have also considered the possibility of improving the quality of the basis by supplementing the 6-31G** basis set by adding a diffuse function (α_c^{sp}= 0.0438, α_{Li}^{sp}=0.0074) (13).

A total energy, Eo, for the lowest vibrational level of a ground electronic state was obtained by adding the zero-point correction, given from a set of harmonic frequency analysis (14),

$$Eo = Ee + D(ZPE)$$

where Ee is the electronic energy at equilibrium. The BSSE was evaluated using the counterpoise procedure of Boys and Bernardi (15), by substracting the counterpoise energy of the unlithiated radical (C_2H_3 or C_2H_5) and the Li^+ ion within the 6-31+G** basis set of the Li^+-radical adduct.

Finally, in order to obtain energies that contain the effects of electron correlation (16), calculations were performed at the MP4SDTQ (full MP4 with single, double, triplet and quadruple substitutions)/6-31+G** level for the optimized geometries.

Results and Discussion

1. Geometry

C_2H_3 Many reports have been published previously (17,18). But, for comparative purposes, brief description is given. The vinyl radical is planar in both its $^2A'$ electronic ground state (Cs structure, a in Fig. 1) and $^2B_2$ excited state (C_{2v} structure, b). The structural features of the electronic ground state are that the $C_1C_2H_5$ angle opens out and the C_1C_2 length shortens significantly, when compared with the values in C_2H_4 (e.g. 134.8° vs 121.8° and 1.328 vs 1.335 A respectively, in C_2H_4 at MP2/6-31G*).

The optimal geometry of the CH_2=CH fragment of complex CH_2=$CHLi^+$ (c) is very similar to that found in the C_2H_3 radical (a); the C=C bond is predicted to be essentially the same as the C_2H_3 vinyl radical (a). The comparisons also show that the radical center angle $C_1C_2H_5$, which opens out substantially from the value in ethylene (e.g. 134.8° vs 121.8° in ethylene a HF/6-31G*), is only slightly changed to 135.8° when Li^+ ion is attached to C_2H_3. The small change in the CH_2=CH geometry is expected on the formation of an electrostatic bond, where the change is some distribution of the charge on the Li^+ and CH_2=CH to enhance the bonding. The biggest change in the structure of CH_2=$CHLi^+$ was a 3.4° twist in the $H_5C_2C_1H_3$ dihedral angle when the Li^+ is present.

C_2H_5 As in the case of the C_2H_3 radical, there is no available experimental geometry for the C_2H_5 radical. In the Cs staggered structure (S) which gives the global minimum, the two hydrogens on the radical center are calculated to be bent 11.4° degrees out of plane. Pakanski and Dupuis (19) have reported Hartree-Fock (UHF) optimal geometries for both the staggered and eclipsed form (E) with essential the same bond lengths and angles as those calculated by us (Table I). Geometric features are that the CC bond length shortens significantly on going from C_2H_5 (S, 1.498 A) to C_2H_3 (a, 1.328 A) and the angles at the C_2 valance center open 128.3° to 134.8°.

Structure changes in C_2H_5 (S) that occur on Li^+ attachment are also followed by the UHF/6-31+G** calculations. The optimized Cs geometry (e) is listed also in Table I. Since a UHF/6-31+G** second-derivative calculation gave all real frequencies, the ground-state potential surface has an energy minimum in this form.

As in the case of $C_2H_3Li^+$, there is no significant change in the CC length of $C_2H_5Li^+$ on lithiation ionization. However, the $C_1C_2X_7$ angle is significantly bent from 168.6 to 155.4°.

Comparisons with $C_2H_3Li^+$ complex indicate that 1) as expected, the C-Li^+ length (2.310A) in structure (e), which is comparable to that (2.309A) calculated for the $C_2H_3Li^+$ cation at the same level of theory, is quite large, 2) the valence angle at C_2 is 109.0°, very much unlike that of $C_2H_3Li^+$ (ca. 80.5°), which is strongly bent.

2. Li^+ affinity

The Li^+ affinity is actually the energies for the R-Li^+ bond dissociation energies (BDE) in R-Li^+ complex. With regard to the Li^+ affinity, Table II shows total energies with inclusion of corrections.

Li^+ affinity of C_2H_3 The electronic ground-state potential surface of C_2H_3 has the global minimum for a planar Cs structure (a) with $^2A'$ electronic state among other possible structures. The excited state is the ethenyl C2v form (b) which is calculated to be 1.19 kcal/mole higher than the most stable form. The lithiation energy (Li^+ affinity) with the bidentate bond formed (c) is calculated to be 4.0 kcal/mol stronger than that with the Li^+ adduct of a planar Cs conformation (d).

Li^+ affinity of C_2H_5 The present UHF/6-31+G** calculations predict that the staggered conformation (S) of the ethyl radical is calculated to lie only 0.13 kcal/mol below the eclipsed one (E), which represents the barrier top of rotation. Compared to previous calculations (20) at the UHF/6-31G** level, the C-C bond distance becomes 0.01 A smaller in both conformations,

while the calculated rotational barrier of 0.16 kcal/mol turned out to be almost the same as the present study. At the UHF/6-31G** level, we find the Li^+ affinity of C_2H_5 to be almost 3.2 kcal/mol *smaller than that of* C_2H_3.

3. Nature of bonding Summary is shown in Table I for the interaction of radical and Li^+ ion, together with values due to Bentley (4). The nature of bonding is evaluated by using Mulliken population analysis. There is a considerably small charge transfer in lithiated species because of the electropositive nature of the alkali metal, i.e. Li^+ is shown to retain 0.72-0.79 electronic units (e) of its positive charge in the adducts. The charge transfer involved in the formation of the Li^+ complex is always smaller than 0.3e. This result demonstrates that bonding is due to mostly to electronstatic interaction, the main contribution of which is made by the ion-dipole attractions.

The Li^+ affinity of the radical (R) is actually the energies for the R-Li^+ bond dissociation energy (BDE) in R-Li^+ complex. The BDEs calculated with all corrections included at the 6-31+G** level are $De(C_2H_3\text{-}Li^+)$ = 20.9 kcal/mol and $De(C_2H_5\text{-}Li^+)$ = 17.1 kcal/mol. These are comparably smaller than the other Li^+ affinities of homologous molecule, which were obtained from the experimental and theoretical study. For example, the Li^+ affinity of C_2H_2 and C_2H_4 has been studied; leading to a theoretical value of 23.6 and 23.2 kcal/mol due to Pople (6) respectively, and to a experimental value of 23 kcal/mol due to Beauchamp for C_3H_6 (11).

Table I. Summary of 6-31+G** total energies (hartree) and Li^+ affinities ΔE(Kcal/mol)

Chemical Species	Hartree-Fock energy (hartree)[a]	Li^+ affinity, ΔE *Literature*[b]	*present*[c]
Li^+	-7.23554		
C_2H_3 (a)	-77.39989		
C_2H_3 (b)	-77.38791		
$C_2H_3Li^+$ (c)	-84.65535	25.6	20.9
C_2H_5(S)	- 78.60753		
C_2H_5(E)	-78.60731		
$C_2H_5Li^+$(e)	-85.86955	20.7	17.1

a) SCF energies with the UHF/6-31+G** basis set.
b) From the MP2/6-31G** studies (Ref. 4).
c) By adding the electron correlation (MP4SDTQ), the zero-point energy (ZPE) and the basis set superposition error (BSSE) corrections.

References

1. Fujii, T. Anal. Chem. 1992, 64, 775.
2. Fujii, T. Chem. Phys. Lett. 1992, 191, 162.
3. Fujii, T.; Shouji. K. Phys. Rev. A 1992, 46, 3555.
4. Bentley, J. Chem. Phys. Lett. 1992, 200, 518.
5. Smith, S. F.; Chandrasekhar, J.; Jorgensen, W. L. J. Phys. Chem. 1982, 86, 3308.
6. Del Bene, J. E.; Frisch, M.J.; Raghavachari, K.; Pople, J. A.; Schleyer, P. R. J. Phys. Chem. 1983, 87, 73.
7. Anvia, F.; Walsh, S.; Capon, M.; Koppel, I. A.; Taft, R. W. de Paz, J. L. G.; Catalan, J. J. Am. Chem. Soc. 1990, 112, 5059.
8. Fujii, T.; Tokiwa, H.; Ichikawa, H.; Shinoda, H. J. Mol. Struc. (Theochem) 1992, 277, 251.
9. Kebarle, P. Ann. Rev. Phys. Chem. 1977, 28, 445.
10. Keesee, R. G.; Castleman, Jr. A. W. J. Phys. Chem. Ref. Data 1986, 15, 1011.
11. Woodin, R. L.; Beauchamp, J. L. J. Am. Chem. Soc. 1978, 100, 501.
12. Gaussian 90, Revision J. M. J. Frisch, M. Head-Gordon, G. W. Trucks, J. B. Foresman, J. S. Binkley, C. Gonzalez, D. J. Defrees, D. J. Fox, R. A. Whiteside, R. Seeger, C. F. Melius, J. Baker, R. L. Martin, L. K. Kahn, J. J. P. Stewart, S. Topiol, and J. A. Pople, Gaussian, Inc., Pittsburgh PA, 1990.
13. Siegbahn, P.E. M.; Yoshimine, M.; Pacansky, J. J. Chem. Phys. 1983, 78, 1384.
14. Pople, J. A.; Schlegel, H. B.; Krishnan, R.; DeFrees, D. J.; Binkley, J. S.; Frisch, M. J.; *Whiteside, R. A.; Hout, R. J.; Hehre, W. J. Int. J.* Quantum Chem. Symp. 1981, 15, 269.
15. Boys, S. F.; Bernardi, F. Mol. Phys. 1970, 19, 553.
16. Krishnan, R.; Frisch, M. J.; Pople, J. A. J. Chem. Phys. 1980, 72, 4244.
17. Sevin, A.; Yu, H. T.; Evleth, E. M. J. Mol. Struct. 1983, 104, 163.
18. Paddon-Row, M. N.; Pople, J. A. J. Phys. Chem. 1985, 89, 2768.
19. Pacansky, J; Dupuis, M. J. Chem. Phys. 1978, 68, 4276.
20. Claxton, T. A.; Graham, A. M. J. Chem. Soc. Faraday Trans. 2 1987, 83, 2307.

Prediction of Hydrological cycle change in a river catchment scale by the coupling of meteorological and hydrological models

Contact Person Akihide Watanabe and Tatsuro Matsuura
Hydrology Division, Public Works Research Institute,
Ministry of Construction.

Keywords hydrological cycle, prediction of precipitation, land surface process, evapotranspiration.

1. Background

During the last decade by-products of men's industrial and agricultural activities were recognized as potential causes for climate change in the form of global warming. These by-products are the gases released into atmosphere. An analysis of the future usage of fossil fuels predicts that the CO_2 concentration will reach twice the pre industrial value by the year 2100. Since an earth surface temperature of 0.5° C has followed a 19% increase CO_2 concentration in the atmosphere, a 100% increase in the CO_2 content by the year 2100 may have serious ramification on the earth surface temperature.

In order to plan countermeasures for hydraulic facilities to cope with the effects of global warming, it is necessary to study the potential long term climate and hydrologic impacts of global warming which may be brought about by the increase of CO_2, at first.

2. Objective

Purpose of this study is to predict hydrological cycle changes due to greenhousegas-induced climate change. But it is more uncertain than prediction of climate change itself, because any climate model does not yield regional climate change such as precipitation and evapotranspiration changes over a river catchment.

One method to solve the problem is to utilize a hydrologic model combined with a meso-scale atmospheric model. We have developed the atmospheric model and have been developing the hydrologic model which incorporate the land surface processes. This model consists of vegetation model, evapotranspiration model and soil moisture model. We tested this model by applying it to Japan region in the winter season.

3. Method

3.1 Atmospheric model

For estimating the distributions of atmospheric variations such as wind velocity vector, temperature and specific humidity, a set of basic equations (Eq. of motion, Conservation Eqs. of mass, thermal energy and water vapor, Hydrostatic Eq.) with a sigma coordinate system are used in the model. A quasi-Lagrangian advective scheme is used to integrate the model. Unlike most other prediction schemes which are based on an Eulerian framework, a second-order accurate scheme in a quasi-Lagrangian frame works is used.

The newest version of this model have two mesh size; large domain model (60km*60km*10layers) and small domain model (20km*20km*12layers) nested by the large one. Using small domain model under global warming scenario and normal climate scenario, we will be able to estimate the change of precipitation due to climate change.

3.2 Land-surface model

As a boundary condition of land surface for atmospheric model, we developed the hydrological model which describe the land-surface process in the balance of heat and water. These land-surface process have a scale much smaller than the horizontal resolution of the meso-scale atmospheric model which is about 10km-100km. As such, it is impossible to resolve the land surface processes in the meso-scale atmospheric model. Therefore, a realistic land-surface parameterization is necessary for the meso-scale atmospheric model. The land-surface model is horizontally averaged.

This land surface model is divided into two processes, which include the heat balance and the water balance. Furthermore the water balance model consist of three models; the vegetation model for water storage intercepted by vegetation, evapotranspiration model from the ground and vegetation, and soil moisture model based on the Green-Ampt formula (Chen et al. 1994). A schematic diagram of the model is as shown in Fig.1. Using these models with atmospheric data, we can know land surface temperature, water content of surface soil layer, evapotranspiration and so on. These give useful information for evaluating the amount of available water resource.

4. Results

4.1 Precipitation simulation by using the large domain model

The annual precipitation calculated by the model under normal climate scenario is shown in Fig.2. In the region over Japan Alps, the annual precipitation is about 3000mm and its value agrees with observed one. However, over Kyushu island the computed annual precipitation is less than observed one. In this 60 km grid size model, the fine features of the historical annual precipitation were still not modeled well. To predict the local features of atmospheric variation, small domain model is suitable for simulation, which will be run in 1994-1995.

4.2 Test of the land surface model

A test run of the land surface moisture model has been carried out with one-way interaction model, in

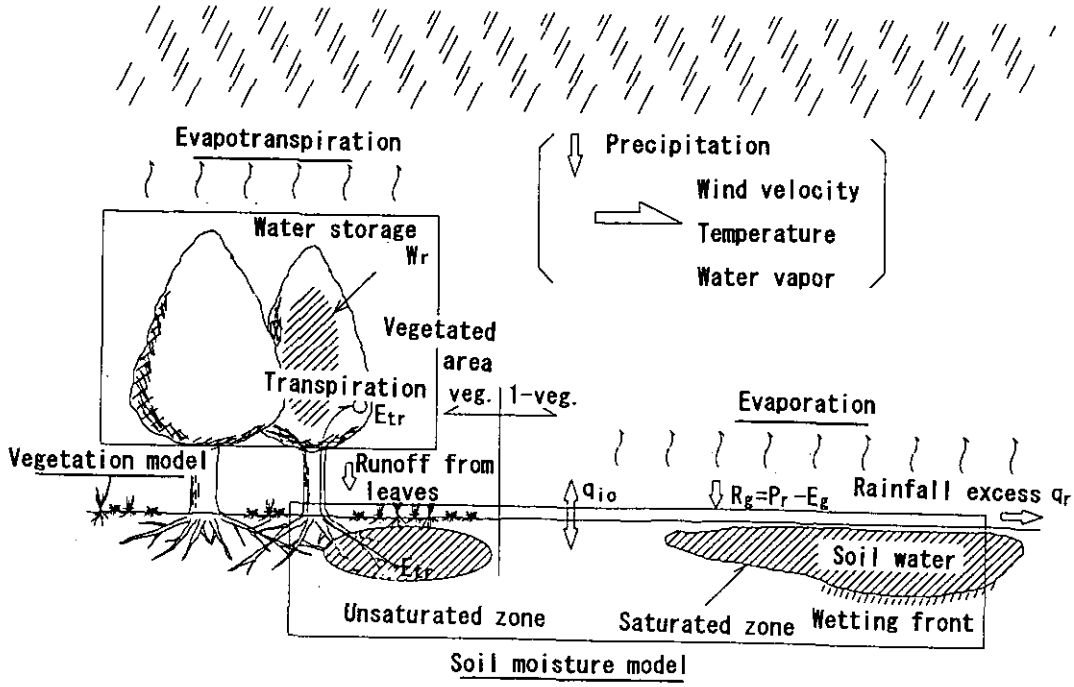

Fig. 1 Concept of hydrological model

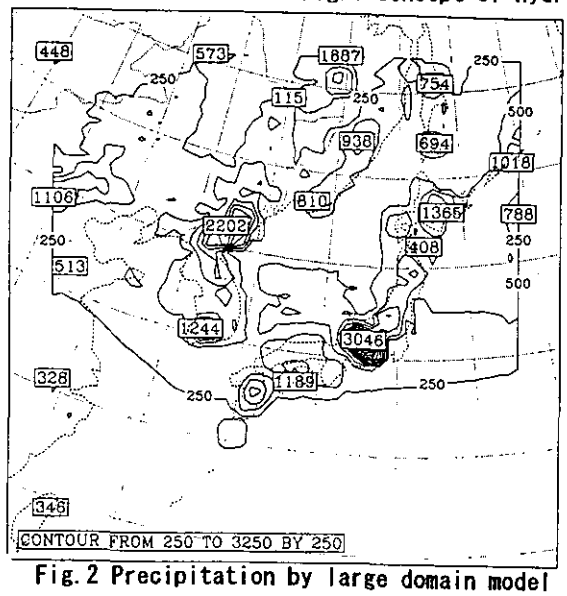

Fig. 2 Precipitation by large domain model

which the calculated results of surface moisture are not utilized in the atmospheric model at present. The month of January 1989 was taken as the test period. The model provides hourly data of precipitation, evapotranspiration surface moisture content and for comparing purpose, the evapotranspiration obtained by the Bowen ratio method.

Fig. 3 presents the mean evolution of the land surface processes averaged over all grids in the small domain model. It is shown that the first precipitation at about 110 hr of the month and reaches its peak at 170 hr of the month. The surface moisture content increases after first precipitation. The evapotranspiration evaluated from land surface model is large when the surface soil is wet enough. Because of active evapotranspiration, moisture content decrease gradually. On the other hand, one evaluated from Bowen ratio method shows almost constant pattern and its intensity is relatively weak .

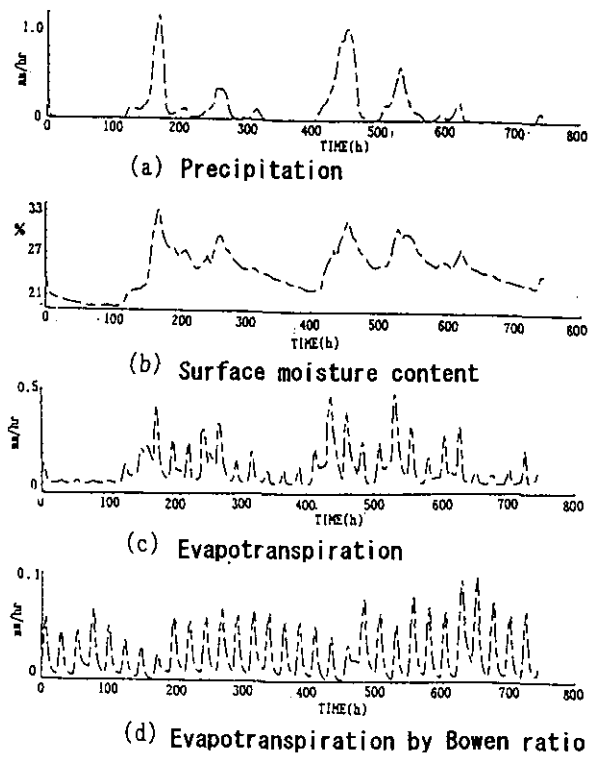

Fig. 3 Land surface process evolution averaged over all land surface in Japan

References

Chen et al.: Spatial averaging of unsaturated flow equations under infiltration condition over areally heterogeneous fields, 1, Development of models, Wat. Res. Res., 30(2), 523-533, 1994.

Chen et al.: Spatial averaging of unsaturated flow equations under infiltration condition over areally heterogeneous fields, 2, Numerical simulation, Wat. Res. Res., 30(2), 535-548, 1994.

SUPERCOMPUTER SX-3 OVERVIEW

Senior manager Naoyuki Takiguchi, Manager Tatsuya Takahama
Assistant manager Akihiro Musa
NEC Corporation,1st C&C Systems Operations Unit
1st Government Systems Division

1.System Configuration

In February 1992 National Institute for Environmental Studies(NIES) installed the SX-3 system,a SX-3/14 with the operating system SUPER-UX. NIES's SX-3 provides a peak vector performance of 5.5 GFLOPS, and has the following features:

- 1 Gbytes of main memory
- 3 Gbytes of extended memory
- 53 Gbytes of magnetic disk capacity
- 28 Gbytes of high speed magnetic disk capacity
- 790Gbytes of mass data processing system
- Ultra Net operated at 800 Mbps.

The mass data processing system (MDPS) and the SX-backstore system were installed in March 1994.The MDPS has 525 optical disk units, a storage capacity of 790 GB. It connects to super-high-speed HIPPI channels and achieves a sustainable data transfer rate of over 8 MB per second. The SX-backstore system is archival file-storage(migration/recall) system of the MDPS.

Fig.1 shows the system configurations with the SX-3 and the other central machines; SUN Server490, SGI Power 4D/310GTX, SGI Power 4D/35TG. The network is based on a FDDI backbone ring connecting the UltraNet with CISCO router. A LANP and Ultra Hub are used to attach the SX-3 to the FDDI.

The NIES-NET is connected to the TISN (Todai International Science Network) by a router, so everyone can get access to the SX-3 upon obtaining authorization together with a password and user-id.

2.SUPER-UX

SUPER-UX is based on UNIX System V and incorporates numerous Berkeley Software Distribution 4.3 (BSD4.3) features. SUPER-UX adds a number of extensions for supercomputers. SUPER-UX produces optimum system performance by providing:

- multiprocessor support
- high-speed input/output
- high-speed swapping using the extended memory unit
- priority scheduling

SUPER-UX also provides efficient operation management through powerfull batch processing, large-scale file support and system freeze/restart. By incorporating many BSD4.3 commands,like networking,SUPER-

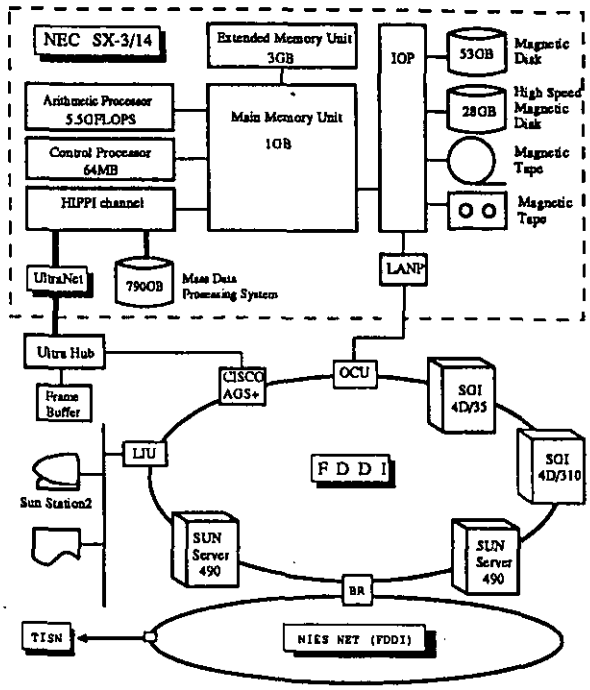

Fig.1 System Configuration

UX provides a substantial,easy-to-use operating system.

1. Multiprocessor/parallel processing support
   SUPER-UX provides true support for multiprocessor and parallel processing which permit an efficient parallel kernel execution. This leads to the high performance characteristics of the total system.
2. High-speed input/output and easy-to-use large-scale file system
   SUPER-UX provides the Supercomputing File System(SFS) for high-speed large-capacity file input/output operations. SFS supports buffer-less input/output,continuous block allocation and large-capacity data transfer, greatly improving file input/output performance. In addition,the Intelligent I/O Accelerator Subsystem(IAS),as a high-speed input/output subsystem,supports the use of the extended memory unit as a disk cache,parallel input/output functions and asynchronous input/output functions.

Virtual volume is a mechanism to systematically handle a wide variety of physical volumes and is incorporated into SUPER-UX. This creates logical volumes of various performance levels and makes it possible to easily configure large-capacity files.

3. Expanded batch processing function
   A batch subsystem based on the Network Queuing System(NQS) supports the production requirements of the supercomputing center. Job class and enhanced scheduling algorithms efficiently control the system workload. SUPER-UX NQS lets both users and operations staff control,monitor and terminate batch jobs. The results of NQS batch submissions are automatically sent to other UNIX systems that use NQS, held as files for interactive retrieval or viewing,or are spooled directly to the system print queue.
   The Remote Queuing System(RQS) can input batch jobs to SUPER-UX from remote IBM's MVS system and execute them.
4. Network File System(NFS) support
   NFS offers distributed file system support that permits access from different operating system environments within the network. This distributed file system provides a remote mount capability based on the client/server model.
5. Enhanced operations management
   - Operation management
     In addition to standard UNIX functions,SUPER-UX operation management includes file space control,job accounting and file backup to simplify system operations.
   - System freeze and restart
     This lets a system interrupt all programs currently executing,store all relevant main memory information into a freeze file and later restore the main memory at the point it was interrupted.
   - Checkpoint-restart function
     This function provides a system capability to interrupt the execution of a program currently in operation at any time and to restart it later. Thus,the function allows flexible system operation,such as top-priority execution of an urgent job and split execution of a long-running job.
   - Automatic operation function
     The Automatic Operation Controller(AOC) enables labor-saving and unattended operation,as well as automatically powering the system up or down.

3.Usage of the SX-3

The usage of the SX-3 resources is monitored and controlled through user administration activities like account application processing, user accounting, etc.

Fig.2 and Fig.3 show the session time and cpu time usage from April 1993 to July 1994.

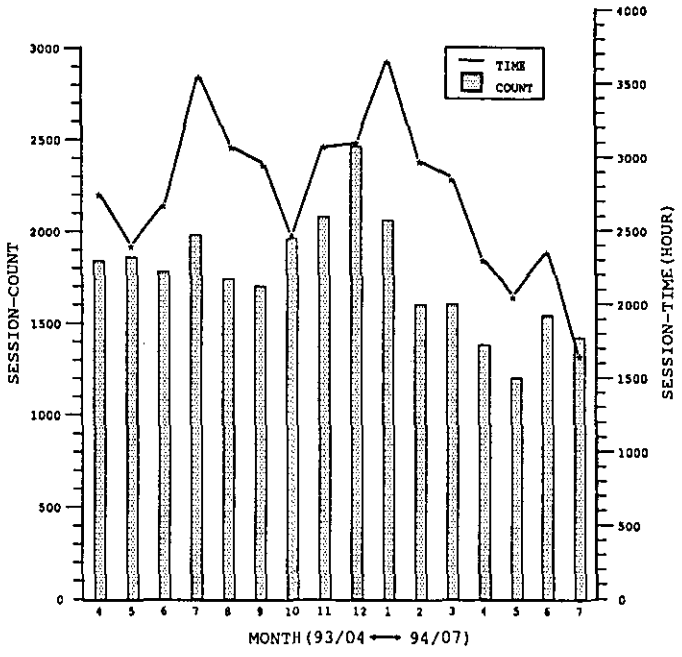

Fig.2 Usage of Sessions

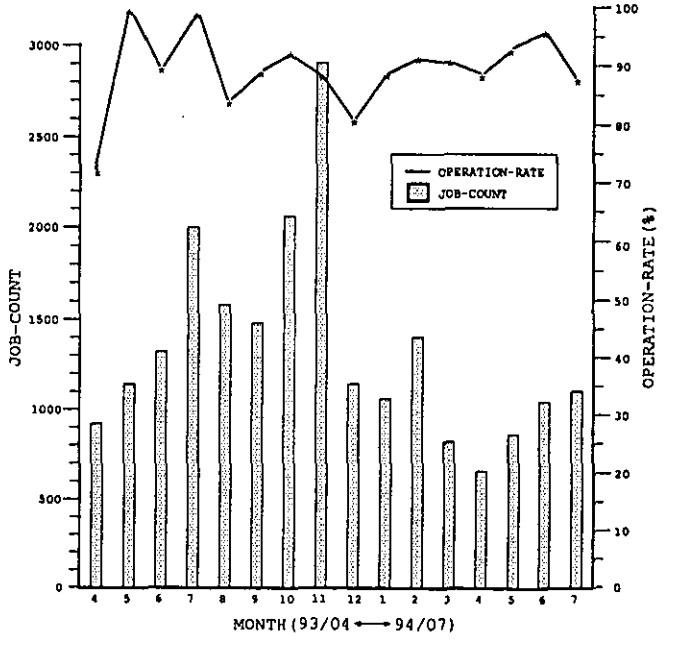

Fig.3 Usage of Jobs